Electronic Supplementary Information

Gel-like Aggregation of Photoluminescent Calcium Phosphate Nanoparticles via Citric Acid Surface-Engineering

Yuhi Kinoshita, [a] Tomoki Isa, [a] Wanyu Shi, [a b] Daichi Noda, [a] Kurisu Mikami, [a] and Motohiro Tagaya [a *]

[a] Department of Materials Science and Bioengineering, Graduate School of Engineering, Nagaoka University of Technology, 1603-1 Kamitomioka, Nagaoka 940-2188, Japan.

[b] Japan Society for the Promotion of Science (JSPS) Research Fellowship for Young Scientists (DC), 5-3-1 Koji-machi, Chiyoda-ku, Tokyo 102-0083, Japan.

**** Author to whom correspondence should be addressed:***

Tel: +81-258-47-9345; Fax: +81-258-47-9300, E-mail: tagaya@mst.nagaokaut.ac.jp

Scheme S1

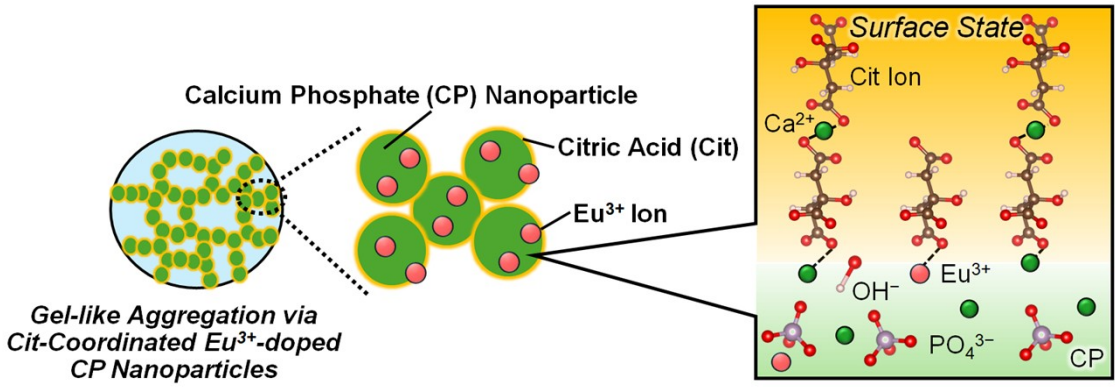

Scheme S1. Illustration of the gel-like aggregation formed via Cit-coordinated Eu^{3+}-doped CP nanoparticles in this study.

Experimental Procedure S1

Based on the reported procedure,[S1] the Cit-coordinated Eu^{3+}-doped CP nanoparticles were synthesized. A phosphate source solution was prepared by dissolving K_2HPO_4 (10 mmol) and Cit (20 mmol) in 70 mL of ultrapure water, and tetramethylammonium hydroxide aqueous solution (TMAOH; 25 vol%) was used to adjust the pH value to be 12.5. Subsequently, a calcium source solution was prepared by dissolving $CaCl_2 \cdot 2H_2O$ (19.5 mmol) and $EuCl_3 \cdot 6H_2O$ (0.5 mmol) in 30 mL of ultrapure water. Both solutions were adjusted to either ***4*** or ***40*** °C, and the calcium source solution was added dropwise to the phosphate source solution at a rate of 1 mL min^{-1} under stirring for 3 h. The resulting suspension was centrifuged (12000 *g*, 4 °C, 5 min) to obtain a white solid phase, which was subsequently washed with ultrapure water and ethanol. The wet solid was redispersed in ultrapure water and diluted to adjust the solid concentration to be 6 wt%.

As the reference sample for FT-IR analysis, the TMA^+-Cit^{3-} species was synthesized according to the previously reported method.[S2] Specifically, Cit was completely dissolved in an aqueous TMAOH (25 wt%) solution at a molar ratio of TMA^+ to Cit^{3-} of 3. The solution was evaporated and dried at 60 °C to obtain the precipitates, which were fully dissolved in ethanol by sonication and subsequently evaporated at 60 °C. The recrystallized compound was designated as TMA^+-Cit^{3-}. In addition, Cit and TMAOH were used as received without further purification.

Reference

S1. Z. Liu, T. Kataoka, S. Samitsu, D. Kawagoe and M. Tagaya, *J Mater Chem B*, 2022, **10**, 396–405.
S2. W. Shi, K. Mikami, I. Yamada, J. Chandra, Z. Liu, Y. Kinoshita and M. Tagaya, Inorg. Chem., 2026, **65**, 191–199.

Experimental Procedure S2

The fluidity of the dispersion was observed by the state of droplets on a titanium plate (AS ONE Corporation, 3-7508-02). In particular, 0.2 mL of ***T-0*** was dropped onto the titanium plate at room temperature, the plate was then immediately placed upright (**Scheme S2(a), ESI**). As a result, both the dispersions clearly exhibited the fluidity. Meanwhile, the dispersion was dropped on a titanium plate and heated at 37.5 °C for 30 min under 94% relative humidity (***S*=*30***). The plate was then placed upright and vibrated (60 Hz, 10 s) to examine the gel-like viscous state (**Scheme S2(b), ESI**). As a result, a gel-like viscous state with the reduced fluidity was clearly observed for ***4-30***, whereas the fluidity was retained for ***40-30***.

Scheme S2

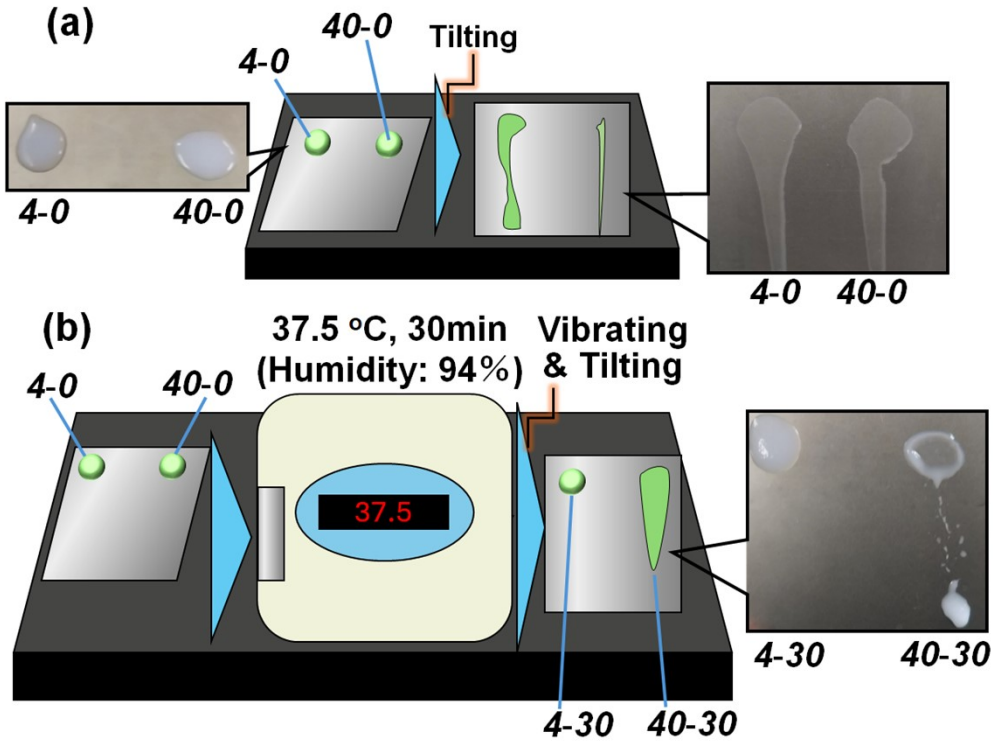

Scheme S2. Illustration of the processes for evaluating (a) the fluidity of ***T-0***, and (b) testing the gel-like state ***T-30***.

Experimental Procedure S3

The hydration state incorporated within the ***T-0*** structure was evaluated by TG-DTA (Rigaku Corporation, TG8120). The TG and DTA curves of ***T-0*** were recorded using an aluminum pan under a nitrogen atmosphere. Subsequently, the weight loss, the integrated areas of the main endothermic peak and the shoulder peak were calculated. The shoulder peak areas were calculated from the DTA curve shown in **Fig. S1(a), ESI**, by taking the temperature range between the zero points in the second-derivative of the endothermic peak curve (**Fig. S1(b), ESI**). The endothermic peak curve within the temperature range was connected by a straight line, and the area corresponding to the shoulder-type endothermic peaks (yellow region) was calculated. In particular, the endothermic peak in the range of 40-105°C was defined as the main endothermic peak (blue region), and its area was calculated. Finally, the percentage (%) of the shoulder-type endothermic peak area (yellow region) to that of the main endothermic peak (blue region) was calculated.

Fig. S1

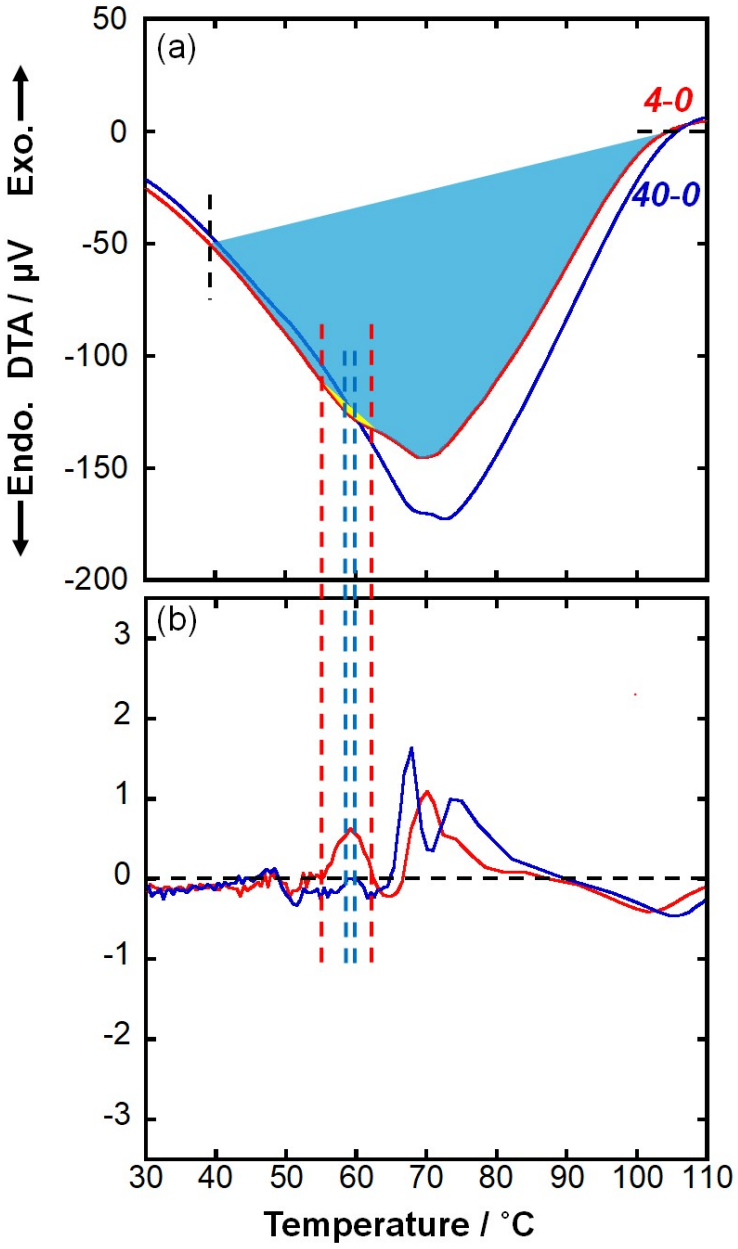

Fig. S1. (a) DTA and (b) the second-derivative curves of ***4-0*** and ***40-0***. Here, the blue area from the onset at 40 °C to the point at which DTA returned to 0, corresponding to the endothermic peak, and the yellow area between the inflection points in the second-derivative DTA curves (i.e., the gelation-like peak) were calculated.

Experimental Procedure S4

0.5 μL of ***T-S*** was dropped on a slide glass, sandwiched by a cover glass and heated under 100% humidity at 37.5 °C for 30 min. Then, the sandwiched sample was frozen by liquid nitrogen for 1 min to maintain the spinodal decomposition state (i.e., metastable phase), and the obtained sample was denoted as ***T-30***-pre-dry. The structure was observed using the optical microscope (CKX41, Olympus Corporation).

Experimental Procedure S5

The nanoparticle shape characterization was performed using a TEM (HT7700, Hitachi High-Tech Corporation) at 100 kV. The samples for the observation were prepared by diluting ***T-S*** in ethanol at 0.01 wt%, casting the dispersion on carbon-coated copper grids and vacuum-drying. In the observed images, the short and long lengths and aspect ratios were measured for 150 nanoparticles, and their average values (*Ave.*) and coefficients of variation (*Cv.*) were calculated.

Experimental Procedure S6

The nanoparticles were dissolved in an aqueous HCl solution (pH = 2), and the solution was measured using the UV-Vis spectroscopy (V-750, JASCO Corporation). The maximum absorbance due to the carboxy groups of the Cit was obtained at 210 nm to determine the coordinated amount of Cit in the Cit/HA nanoparticles. Then, the standard calibration curve of Cit was fitted to calculate the coordinated amount of Cit (**Fig. S2, ESI**). The specific surface area was measured using a nitrogen (N_2) adsorption and desorption instrument (BELSORP-miniII, MicrotracBEL Corp.) at −196 °C, and the samples were pretreated at 120 °C for 1 h under vacuum conditions. The Brunauer–Emmett–Teller (BET) surface areas (S_{BET}) were used to calculate the molecular occupancy of Cit on the nanoparticles by the following **Eq. S1**.

$$\text{Molecular occupancy of Cit (\%)} = \frac{A \times C \times N_A}{10^{19} \times S_{BET}} \qquad (\textbf{Eq. S1})$$

Where A is the coverage area of a unit Cit molecule on NPs (0.166 nm^2), C is the coordinated amount of Cit and N_A is the Avogadro constant. As a result, C = 1.264 $mmol \cdot g^{-1}$ and S_{BET} = 244 $m^2 \cdot g^{-1}$ for ***4-0*** and C = 0.715 $mmol \cdot g^{-1}$ and S_{BET} = 282 $m^2 \cdot g^{-1}$ for ***40-0*** were determined, and these values were used to calculate the molecular occupancy of Cit.

Fig. S2

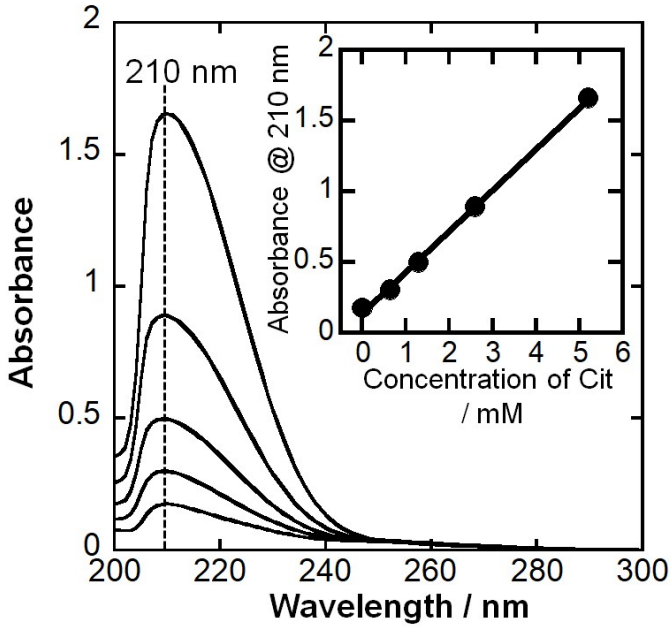

Fig. S2. UV-Vis absorption spectra of the Cit aqueous solution at pH of 2. Inset: linear-calibration plot between the Cit concentration and absorbance (R^2= 0.9995).

Experimental Procedure S7

The crystal structures of ***T*-*S***-dry were analyzed by XRD (SmartLab, Rigaku Corporation) using CuKα radiation (λ = 1.5418 Å) at 40 kV and 30 mA, with a scan speed of 3.0° min^{-1}, a step size of 0.01°, and continuous scan mode. The diffraction peak positions, angles, and full widths at half maximum were obtained using the instrument software (SmartLab Studio II, Rigaku Corporation). The crystalline phases were identified according to the ICDD standard database by the Hanawalt method. The profile fitting was carried out using the SmartLab Studio II software package. This procedure refines the crystallographic parameters by least-squares fitting of theoretical peak profiles to the measured data. The refinement of diffraction patterns was performed with a pseudo-Voigt function (**Eq. (S2)**).

$$f(x) = Aexp\left(-\frac{(x-B)^2}{C^2}\right) + (n-1)\left(\frac{AC^2}{(x-B)^2 + C^2}\right) \quad (\mathbf{S2})$$

Here, ***A*** is the peak intensity, ***B*** is the peak position, and ***C*** is the peak broadening.

The chemical bonding states of ***T*-*S***-dry were examined by FT-IR spectroscopy (FT/IR-4600 type A, JASCO Corporation) in diffuse reflectance mode. The background spectra were recorded using KBr powder, with a spectral range of 4000-400 cm^{-1}, 128 scans, and a resolution of 4.0 cm^{-1}. The samples were prepared as diluted powders by mixing each sample with KBr at a ratio of 1:20. The obtained spectra were corrected by removing the contributions of atmospheric H_2O and CO_2 and by applying baseline correction over the 4000-400 cm^{-1} region. The measured diffuse reflectance (R_∞) was converted into Kubelka-Munk (KM) units using (**Eq. (S3)**).[S3]

$$\frac{K}{S} = \frac{1 - R_\infty}{2R_\infty} \quad (\mathbf{S3})$$

Here, *K* is the absorption coefficient and *S* is the scattering coefficient, where S was assumed to be constant because of its weak wavenumber dependence.

Reference

S3. G. Kortüm, W. Braun and G. Herzog, *Angewandte Chemie International Edition in English*, 1963, 2, 333–341.

Experimental Procedure S8

The PL properties were evaluated by luminescence spectroscopy. The luminescence spectra were recorded on the FP-8500 spectrophotometer (JASCO Corporation) with an excitation wavelength of 394 nm using a Xe lamp (atmosphere: air, excitation/detection slit sizes: 2.5 nm/2.5 nm, measure time: 0.1 s, step width: 1.0 nm).

The PL intensity ratios for ***T-S*** were calculated as follows. The emission intensity of the $^5D_0 \rightarrow {}^7F_1$ transition, assigned to the magnetic dipole transition of Eu^{3+}, is scarcely influenced by the surrounding coordination environment, whereas that of the $^5D_0 \rightarrow {}^7F_2$ transition, arising from the electric dipole transition, is strongly dependent on the local symmetry around Eu^{3+}. Accordingly, the $^5D_0 \rightarrow {}^7F_2$ transition has been reported to be observed more strongly in low-symmetry environments for Eu^{3+} than in high-symmetry environments.[S4] Accordingly, the ratio of the integrated intensity of the $^5D_0 \rightarrow {}^7F_2$ transition (I_{614}, 603-630 nm) to that of the $^5D_0 \rightarrow {}^7F_1$ transition (I_{590}, 577-603 nm), i.e., I_{614}/I_{590}, was calculated. In addition, the $^5D_0 \rightarrow {}^7F_0$ transition was measured with the excitation/detection slit sizes adjusted to be 1.0 nm/1.0 nm, and the PL peak position was determined by second-derivative analysis.

The emission photographs were recorded under UVA irradiation (FLL365-SD, OPTOCODE CORPORATION, 27 W twin tube, 365 nm).

Reference

S4. K. Binnemans, *Coord Chem Rev*, 2015, **295**, 1–45.

Fig. S3

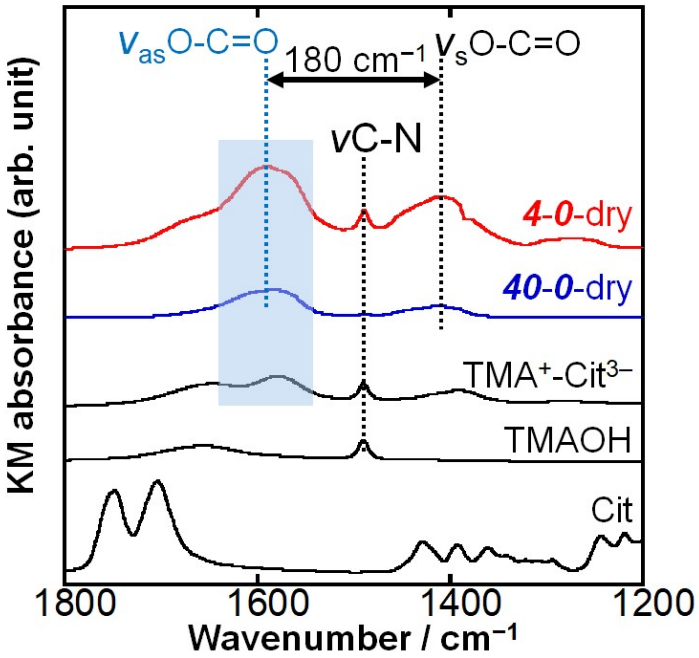

Fig. S3. FT-IR spectra of ***T*-*0***-dry and the reference (TMA^{+}-Cit^{3-}, TMAOH, Cit) at 1800–1200 cm^{-1}.

Fig. S4

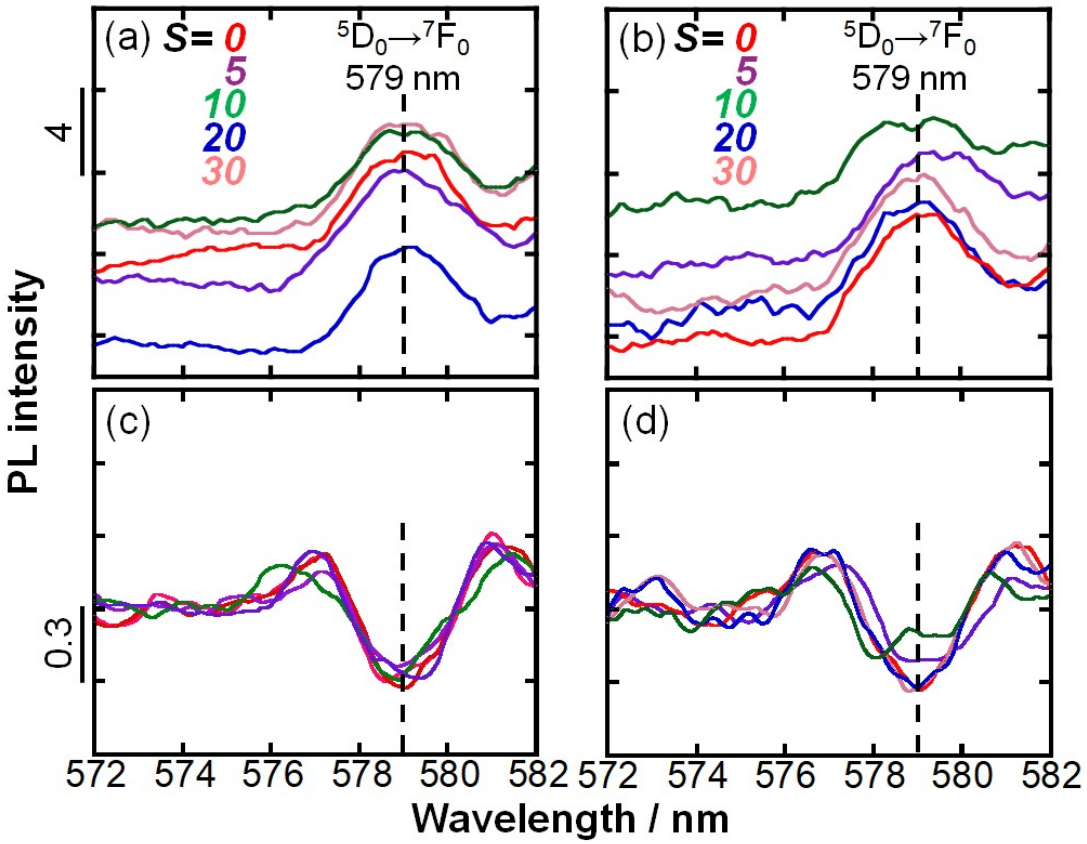

Fig. S4. (a, b) PL spectra of the $^5D_0 \rightarrow {}^7F_0$ transitions and (c, d) the second-derivative spectra for (a, c) ***4-S*** and (b, d) ***40-S*** under excitation at 394 nm.

Scheme S3

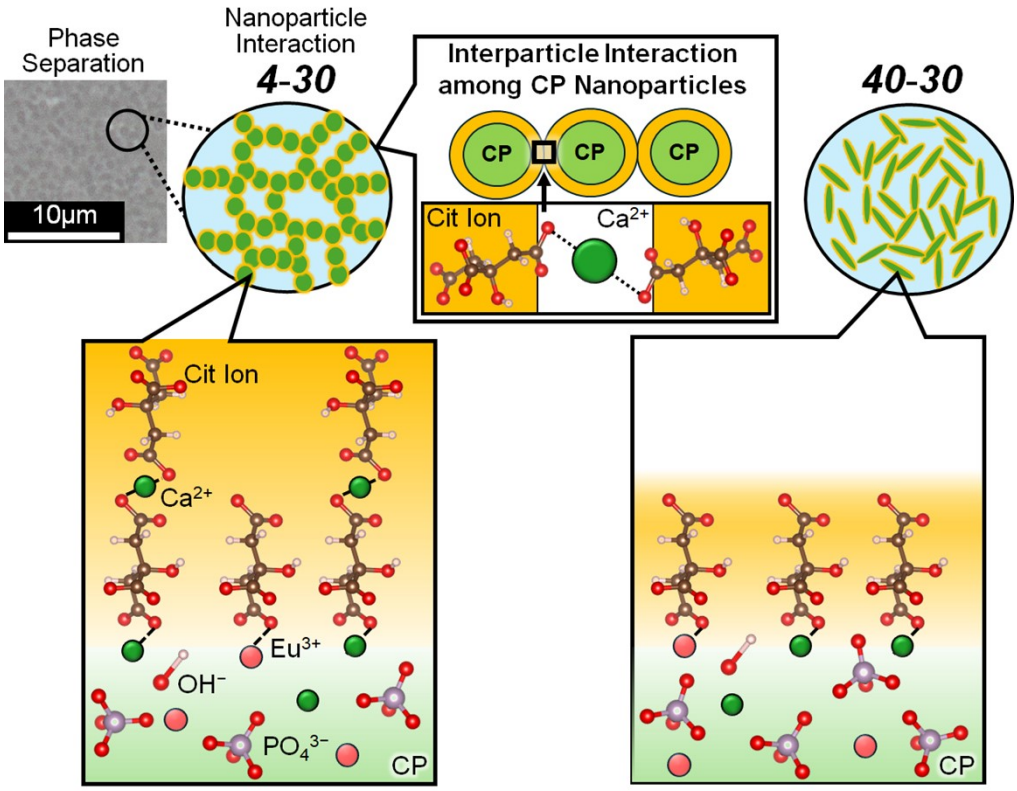

Scheme S3. Illustration of the possible nanoparticle surface states of ***4-30*** and ***40-30*** after heating for 30 min.